Appl Phys B (2011) 102: 123–132
DOI 10.1007/s00340-010-4200-x

Applied Physics B
Lasers and Optics

Measurement of water film thickness by laser-induced fluorescence and Raman imaging

D. Greszik · H. Yang · T. Dreier · C. Schulz

Received: 29 March 2010 / Revised version: 16 July 2010 / Published online: 16 September 2010

Abstract We present two non-intrusive, laser-based imaging techniques for the quantitative measurement of water fluid film thickness. The diagnostics methods are based on laser-induced fluorescence (LIF) of the organic tracer ethyl acetoacetate added to the liquid in sub-percent (by mass) concentration levels, and on spontaneous Raman scattering of liquid water, respectively, both with excitation at 266 nm. Signal intensities were calibrated with measurements on liquid layers of known thickness in a range between 0 and 500 µm. Detection via an image doubler and appropriate filtering in both light paths enabled the simultaneous detection of two-dimensional liquid film thickness information from both methods. The thickness of water films on transparent quartz glass plates was determined with an accuracy of 9% for the tracer LIF and 15% for the Raman scattering technique, respectively. The combined LIF/Raman measurements also revealed a preferential evaporation of the current tracer during the time-resolved recording of film evaporation.

1 Introduction

Surface film formation is a common phenomenon in many practical processes ranging from, e.g. spray cooling in fire fighting applications or cooling of electronic equipment [1] to fuel films in internal combustion engines. In many applications a quantitative measurement of film thickness is desirable in order to optimize injector design and to provide validation data for simulations. Many measurements have focused on hydrocarbon-based liquids such as fuels in engines where wall wetting leads to soot formation and lubricant dilution. For water-based systems, e.g., the injection and evaporation of water-based urea solutions in the exhaust gas stream of Diesel engines during the selective catalytic reduction (SCR) of NO_x is of current interest [2].

For liquid fuels a variety of measurement techniques for the determination of the amount of liquid deposited on surfaces and its respective layer thickness have been developed for applications in internal combustion engines. Techniques relying on mechanical and/or thermodynamic principles make use of, e.g., the change of heat transfer during evaporation of the liquid mass, which leads to a corresponding temperature drop in the wall section covered by the film. In many applications non-intrusive optical in-situ measurements are desirable. Evers et al. [3] used a light cone formed by optical fibers placed in a circle, which is coupled into the liquid layer and measured the recollected light that is due to total internal reflection at the film surface. The detected signal intensity varies with film thickness due to the varying amount of totally reflected light with layer thickness, which is detected through a centrally mounted receiving fiber. Hurlburt et al. [4] and later Shedd et al. [5] used as a measure for film thickness the spatial separation between the location of a light cone launched into the liquid layer and the closest point where internally, totally reflected rays leave the sample and detected with a CCD-camera detector. As an addition to these point measurements, Drake et al. [6] determined the spatial distribution of the liquid fuel mass deposited on a roughened quartz window from the intensity variation in the back scattering of light illumination once the grooves in the surface are partially filled with liquid that is almost matching the refractive index of the surface material.

D. Greszik (✉) · H. Yang · T. Dreier · C. Schulz
IVG, University of Duisburg-Essen, Lotharstr. 1, 47057 Duisburg, Germany
e-mail: daniel.greszik@uni-due.de
Fax: +49-203-3793087

Spectroscopic methods, such as fluorescence or absorption have widely been employed when measuring fluid film thickness. Felton et al. [7], using pulsed ultraviolet (UV) illumination of commercial gasoline at 355 nm from a frequency-tripled Nd:YAG laser and detection of the laser-induced fluorescence via an intensified CCD camera, acquired two-dimensional maps of liquid fuel film thickness in the intake port of an internal combustion (IC) engine, once separate calibration of the signal intensity as a function of film thickness was performed. Kull et al. [8] visualized liquid gasoline fuel films on the inside of a quartz ring that was inserted for optical access as part of the cylinder liner. They used a beam at 308 nm from a XeCl-excimer laser for excitation of commercial fuel. The laser beam coupled into the quartz ring was guided to the liquid film by total internal reflection inside the quartz ring exciting fluorescence in the liquid layer. Alonso et al. [9] coupled a 266 nm laser beam through a quartz plate into a liquid film of iso-octane beyond the critical angle, and measured liquid layer thickness through the fluorescence intensity induced in 3-pentanone as a tracer (10% by volume). The light enters the fuel film from below but is totally reflected at the liquid-air interface as long as its surface is sufficiently flat. This technique avoids signal contributions from air-borne droplets present above the film. Hentschel et al. [10] used 2,3-hexanedione (4%) in a non-fluorescing surrogate fuel (iso-octane) for determining the film thickness at one point with a fiber-based excitation/detection system that was flush-mounted into the wall with argon-ion laser excitation at 457.9 nm.

Concerning water films thickness measurements were mostly performed pointwise for the detection of temporal variations of film thickness, whereas imaging techniques were only used for the investigation of non-evaporating films.

Absorption of visible light from a diode laser at 635 nm and detection of the transmitted beam by a photodiode through a flowing liquid film was used by Mouza et al. [11] when determining the layer thickness down to 1 mm of a water channel flow doped with methylene blue as a tracer. Absolute film thicknesses were obtained from calibration measurements. Similarly, Wittig et al. [12] used NIR laser radiation at 1523 nm to measure the film thickness of pure water in a rectangular duct. Discrimination against light attenuation caused by other effects (e.g., windows) was accomplished by simultaneously recording the transmission of a second laser beam at 633 nm.

The film thickness of a heated, evaporating water layer placed on a transparent wall in the thickness range between 0 and 1000 µm was determined by Yang et al. [13] using two NIR diode lasers at wavelengths of 1392 and 1469 nm, which are non-resonant with any water vapor transition. Additionally, water vapor temperature above the layer was obtained from two-line thermometry using a third laser resonantly tuned through water transitions together with the 1392 nm laser.

Schagen et al. [14] determined temperatures and film thickness from the phosphorescence decay time and fluorescence intensity, respectively, of biacetyl dissolved in a falling wall-wetting liquid water film in the 0.4–2.5 mm thickness range.

In the present article we demonstrate a LIF technique for the two-dimensional imaging of evaporating water film thicknesses and the simultaneous use of Raman scattering and tracer-based LIF. Ethyl acetoacetate was selected as an adequate tracer substance, since its evaporation characteristics adequately match those of liquid water. The advantage of the LIF over Raman technique is its higher signal strength, while Raman scattering is a tracer-free method and therefore independent of problems that can be caused by preferential evaporation of one of the respective compounds. The simultaneous detection may be used to combine the advantages of both techniques, and demonstrate the potentials for non-intrusive layer thickness imaging of temporally and spatially resolved liquid films for practical applications.

2 Spectroscopic background

2.1 Laser-induced fluorescence of tracer species

Laser-induced fluorescence (LIF) is frequently used for measurements of species concentrations in the gas and the liquid phase. With fixed frequency UV laser radiation various small ketone-like or aromatic tracer species can be excited efficiently within their broad unstructured absorption bands. Excitation with spatially expanded laser beams and detection with intensified CCD cameras allows the determination of two-dimensional maps in a variety of combustion situations [15, 16] with high spatial and temporal resolution. A review on tracer LIF fundamentals and applications for gas-phase measurements is given in [17]. For the visualization of non-fluorescing liquids similar tracer species or dye molecules are added in small amounts (typically less than 5% by volume). The emitted fluorescence radiation usually is red-shifted and can be separated from the elastically scattered laser light by suitable filters.

In the experiments described below a frequency-quadrupled Nd:YAG laser at 266 nm provides the excitation source. Since pure liquid water does not fluoresce when excited at this wavelength a suitable tracer is added. The intensity of the induced fluorescence signal, I_{LIF},

$$I_{\mathrm{LIF}} = \eta\phi E_0 N_{\mathrm{tr}} \sigma_{\mathrm{abs}} A d \tag{1}$$

depends on the efficiency of the detection system η, the quantum efficiency ϕ, the temperature- and wavelength-dependent absorption cross section σ_{abs} of the sample and

the number of tracer molecules N_{tr} within the excitation volume (assumed to be formed by the illuminating beam cross section A and the film thickness d) [18].

2.2 Raman scattering

The Raman band shape of OH-stretch vibrations of liquid water is located at Stokes wavenumber shifts between 3200 and 3600 cm^{-1} [19] and is considerably broader and shifted towards smaller wavenumbers as compared to the vapor phase (3550–3650 cm^{-1}) [20]. When excited at 266 nm and with the low spectral resolution in the present experiments (see below) this gives rise to a characteristic peak centered at around 294 nm. In the present work we exploit the intensity of this spectral feature as a tracer-free indicator of film thickness in liquid water.

The scattered Raman signal intensity, I_{Raman}, collected in a small solid angle $d\Omega_{det}$ from a species with concentration N in the sample volume $V = Ad$ can be written as [18]:

$$I_{Raman} = E_0 N \eta \frac{d\sigma_{Raman}}{d\Omega} d\Omega_{det} A d \quad (2)$$

In this equation E_0 is the intensity of the incident laser light, η describes the overall optical efficiency of the detection system in the detecting solid angle $d\Omega_{det}$, and $d\sigma_{Raman}/d\Omega$ is the differential Raman scattering cross section of liquid water. For the latter, Gregory et al. [21] report a value of 1.8×10^{-28} $cm^2/(sr\,molecule)$ at 266 nm. For quantitative evaluation of the spectrally integrated Raman signal, the number of molecules n inside the sample volume can be calculated from $\rho N_A/M$, where ρ, and M are the density and molar mass of liquid water, respectively, and N_A is Avogadro's constant.

Compared with the tracer-LIF method, an obvious advantage of the Raman technique is the detection of a signal without adding a tracer to the solvent, while generally the signal strength is low. In the following, the potentials of the combined application of the LIF and Raman scattering approach for practical liquid water thickness measurements is explored.

3 Experimental

Liquid water films on a quartz window were illuminated from the bottom with a frequency-quadrupled Nd:YAG laser at 266 nm with a pulse energy of 9 ± 1 mJ, recorded by a photodiode, at a repetition rate of 10 Hz. The laser beam is expanded with a lens ($f = -100$ mm) to generate a divergent cone that illuminates an area with 30 mm diameter. The signal was collected in backward direction through the quartz plate and reflected by an aluminum mirror towards an intensified CCD camera (LaVision, StreakStar) fitted with a

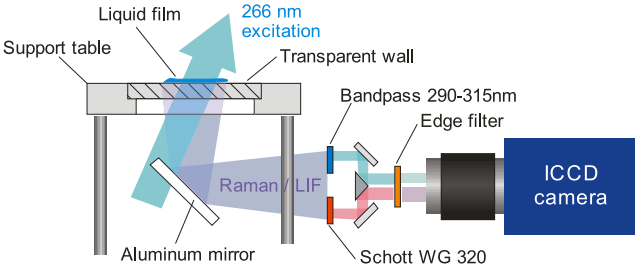

Fig. 1 Setup for two-dimensional Raman and LIF imaging of liquid films on a quartz plate with two optical detection channels

UV lens (Coastal Optics, 105 mm focal length, $f_\# = 4.5$). To simultaneously detect tracer LIF and Raman scattered light from the same spatial regions on separate areas on the CCD-chip an image doubler (LaVision) was attached in front of the camera lens and each channel fitted with appropriate filters (cf. Fig. 1). For the Raman detection channel a bandpass filter (Laser Components, BP290–315) was used. The separation of tracer fluorescence from unwanted signal in the LIF channel was performed with a Schott WG320 color glass filter. In addition, for both channels elastically scattered laser light was suppressed with an edge filter (Semrock, RazorEdge 266RS) with an optical density of 6 at the excitation wavelength mounted between image doubler and camera lens.

Liquid layers were prepared by one of two different methods. The first was by dripping small droplets onto the quartz plate using a glass pipette. The droplet shape and liquid layer thickness were modified arbitrarily by spreading the deposited liquid through gentle mechanical stirring. In the second method a commercial 3-hole injector (BOSCH) was directed towards the quartz plate. The respective liquid was ejected with a pressure of 5 bar maintained by a constant nitrogen back pressure and directed towards the plate normal at an angle of 45° from a distance of 50 mm. Single injection events were initiated with a rectangular trigger pulse from a pulse generator sent to the solenoid valve. For time-resolved thickness measurements the evaporation rate of the water film was enhanced by heating the quartz plate from below via a continuous hot air flow from a heating fan. In these cases a thermocouple immersed into the liquid indicated a temperature of approx. 60°C during the course of data recording.

3.1 Calibration tool

For thickness-dependent signal intensity calibrations a tool was designed similar to suggestions described in [10, 11] (Fig. 2). It provides liquid layers of adjustable thickness between two plane-parallel quartz plates. One of the plates is glued into a stainless steel trough filled with the respective liquid. The second one is fixed to an adjustable kinematic

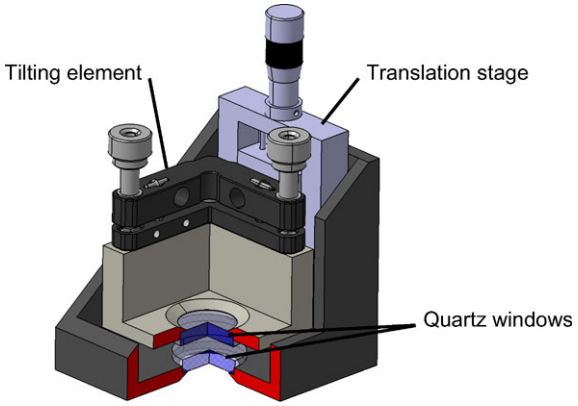

Fig. 2 Calibration tool

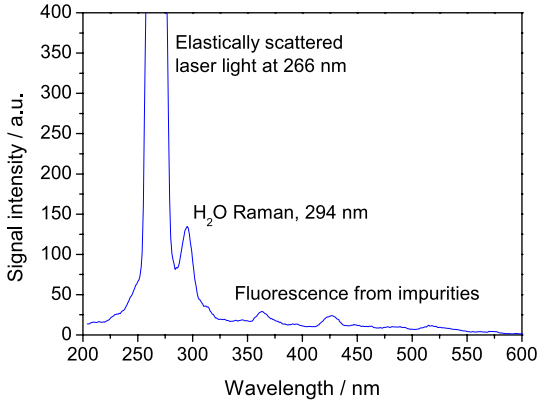

Fig. 3 Fluorescence/Raman spectrum of tri-distilled liquid water obtained from a cuvette with a pathlength of 10 mm; excitation wavelength is 266 nm

holder mounted on a translation stage and positioned above the bottom plate. Its distance relative to the bottom plate was known from the reading of a caliper (accuracy 2 µm, not shown in Fig. 2). The relative parallel orientation of the inner quartz plate surfaces was adjusted using the partial surface reflections on a distant screen from a HeNe-laser beam directed through both plates. Signal intensity vs. film thickness for each optical technique is easily done by replacing the quartz plate in Fig. 1 by the calibration tool without changing any alignment in the excitation/detection channels.

4 Results

4.1 Tracer characterization

The spectroscopic properties of pure water and water/tracer mixtures were investigated in rectangular quartz cuvettes in absorption and fluorescence spectrometers (Varian, Cary 500 Scan and Cary Eclipse, respectively) with a spectral resolution of 2 nm for the absorption and 5 nm for the fluorescence measurement. The absorption of liquid water at 266 nm is negligible. The absorption cross section ($\sigma_{abs} = 4.1 \times 10^{-25}$ cm^2/molecule) was calculated from absorbance data from Hale et al. [22]. It is six orders of magnitude smaller than the absorption cross section of the used tracer (Fig. 4). Fluorescence spectra of tri-distilled water (excitation wavelength: 266 nm) are depicted in Fig. 3 in the spectral range between 200–600 nm. Except for the strong peak from the elastically scattered excitation light and the much weaker peak that is attributed to Stokes-shifted Raman scattering a weak broadband background can be detected in the range between 350 and 450 nm that is attributed to impurities within the sample.

A fluorescent tracer needs to fulfill a number of requirements. The tracer must be water soluble and should not significantly alter the thermo-physical properties of the liquid under investigation. Additionally, it should co-evaporate with the liquid of interest in the relevant temperature range to prevent a variation in tracer concentration in the sample during evaporation. The concentration that is required to generate sufficiently strong signal levels must be low enough to avoid laser attenuation within the expected layer thickness, which can best be achieved by a tracer with a high fluorescence quantum efficiency. The temperature dependence of the absorption and fluorescence spectrum in the investigated range should be moderate or known.

Non-evaporating tracers such as dye molecules must be ruled out because of their accumulation in evaporating systems. We investigated the evaporation behavior of mixtures of water doped with small amounts of different evaporating tracer species representatives of alcohols, ketones and acetates. These included ethyl acetoacetate (EAA), benzyl alcohol, 2-butanone and cyclohexanone. Room temperature liquid-vapor equilibrium calculations of multicomponent mixtures were performed based on the UNIFAC model [23] which led to the conclusion that the tracer whose evaporation behavior best follows that of water needs to have a significantly higher boiling point than the solvent. The calculations had shown that all hydrocarbon-based tracers evaporate preferentially from the mixture. To reduce the volatility, heavy molecules with a high boiling point had to be used. Because of their high volatility, fluorescent species commonly employed as tracers in hydrocarbon fuels, such as acetone, are poor tracer candidates for water.

Taking all previous considerations into account, from the listed tracer species EAA appears as the most suitable tracer to quantitatively characterize—after suitable calibration—liquid water film thickness by its fluorescence signal. Some thermodynamic properties of this species are listed in Table 1.

As shown in Fig. 4, EAA exhibits adequate absorption in the ultraviolet spectral range with an absorption cross section at 266 nm two times larger than that of acetone. Xu et al. [24] determined an absorption cross section of

Table 1 Physico-chemical properties of ethyl acetoacetate and acetone [25, 26]

Property	Ethyl acetoacetate	Acetone
Molar mass	130.13 g/mol	58.08 g/mol
Boiling point	180–181.2°C	55.8–56.6°C
Density	1.0246 g/cm^3 (20°C)	0.79 g/cm^3 (20°C)
Vapor pressure	0.1 kPa (20°C)	24.7 kPa (20°C)
Water solubility	125 g/l (16°C)	Miscible

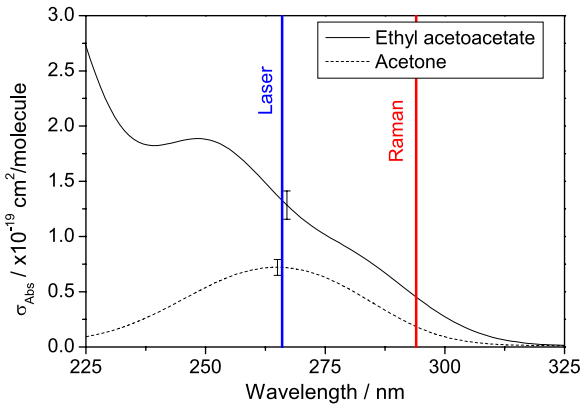

Fig. 4 Measured wavelength-dependent absorption cross section of acetone and ethyl acetoacetate in aqueous solution. The spectral positions of the excitation laser and the induced Raman band of liquid water, respectively, are indicated by *vertical lines*. The spectra was measured in a cuvette with 10 mm pathlength

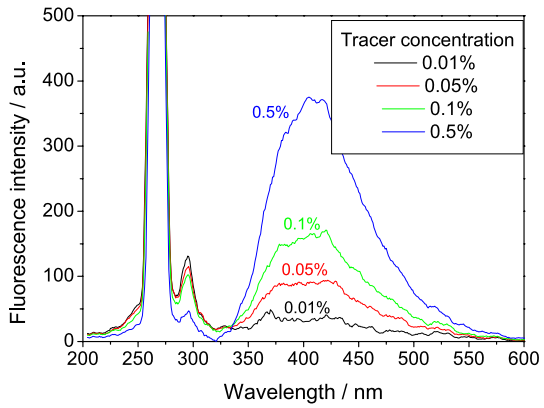

Fig. 5 Fluorescence spectra of ethyl acetoacetate/water solutions at four different tracer concentrations (wt%). The spectra were measured in a cuvette with 10 mm pathlength

0.66×10^{-19} cm^2/molecule at 266 nm, approx. 8% smaller than our value.

EAA fluorescence in water excited at 266 nm (Fig. 5) appears in the 320–550 nm range and therefore can be easily separated from elastically scattered laser light with standard color glass filters (e.g., Schott WG 320).

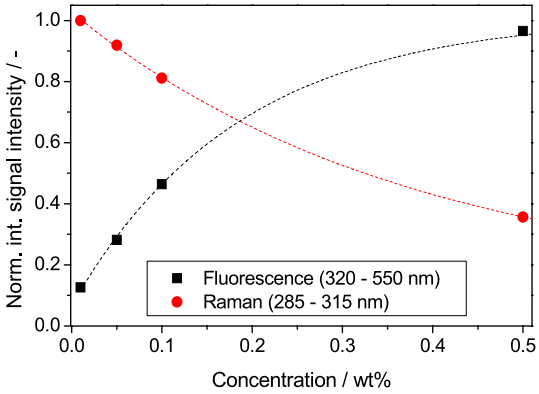

Fig. 6 Normalized fluorescence (spectrally integrated between 320 and 550 nm) and Raman (spectrally integrated between 285 and 315 nm) intensity vs. tracer concentration determined from the spectra in Fig. 5. The *dotted lines* are fits to the data points

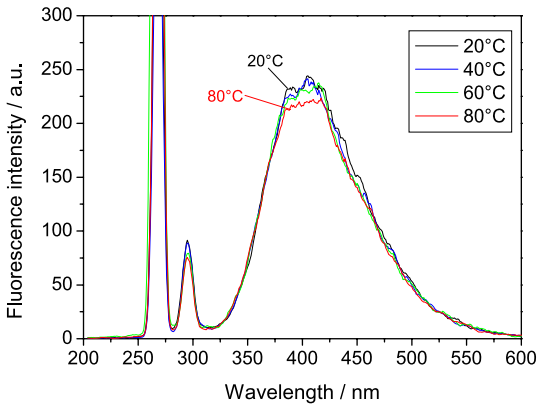

Fig. 7 Temperature dependence of fluorescence spectra of 0.1 wt% ethyl acetoacetate in water (the signal peak around 294 nm is due to vibrational Raman of H_2O)

Figure 6 shows the spectrally integrated signal normalized on the highest signal strength for the fluorescence and Raman detection channel, respectively, as a function of tracer concentration. After a linear increase of the fluorescence signal intensity a plateau region is approached at the highest employed concentration levels. In this region laser attenuation is strong enough that a homogeneous illumination of the sample volume along the absorption pathlength is no longer feasible. The decrease of Raman signal peak with increasing tracer concentration is supporting this conclusion, since less laser light is available for Raman excitation due to attenuation by absorption. In addition, absorption of Raman scattered light at 294 nm by the tracer occurs that also increases with increasing tracer concentration.

As Fig. 7 shows the fluorescence spectra of EAA in water are slightly temperature dependent. With increasing temperature the fluorescence intensity decreases, which is most prominent around the peak of the unstructured band at 400 nm.

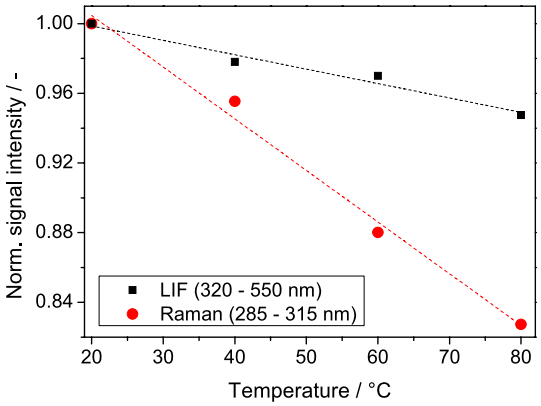

Fig. 8 Signal intensity (integrated between 320 and 550 nm for LIF, and between 285 and 315 nm for Raman scattering) vs. temperature of the liquid. Values are normalized to room temperature; the *dotted lines* are linear fits to the data points

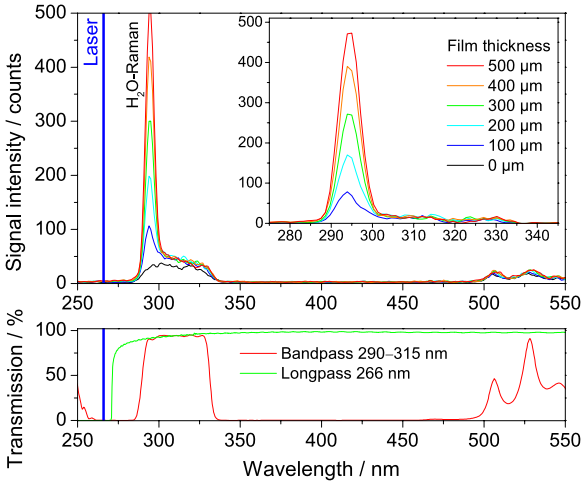

Fig. 9 Spectrally resolved emission in the Stokes-shifted wavelength range of a 0.1% EAA/water solution as a function of layer thickness. *Inset*: Raman signal after subtracting the background spectrum obtained with both quartz plates in contact (i.e., no fluid film). The transmission curves of the optical filters placed in front of the camera lens are depicted in the lower part of the diagram

As shown in Fig. 8, a weak decrease of the spectrally integrated fluorescence intensity of 3% in the temperature range from 20 to 60°C is observed, which in the following is neglected during data post processing. A temperature-dependent spectral shift was not found within this temperature interval. The Raman intensity shows a decrease of 12% at 60°C relative to 20°C. Since the temperature during evaporation is nearly constant this effect could be regarded in the calibration and afterwards neglected in the evaluation.

4.2 Raman intensities

To verify the dependence of the spectrally integrated Raman signal on film thickness spectrally dispersed measurements with water films of a defined thickness were performed using the calibration tool. The signal radiation was focused with a $f = 105$ mm, $f_\# = 4.5$ lens (Coastal Optics, identical to that used for the imaging setup) onto the entrance slit (opening width 200 µm) of an imaging spectrometer (SpectraPro, Mod. 2150i), spectrally dispersed with a 300 lines/mm grating (spectral resolution 2.5 nm) and detected with an ICCD camera (LaVision, StreakStar). The filter combination used for the Raman imaging measurements (Fig. 1) was also placed in front of the spectrometer. The filter transmission curves are depicted in the lower part of Fig. 9. They combine a high transmission in the desired Stokes wavelength range with a sufficient suppression of unwanted signal contributions from elastically scattered laser light and tracer fluorescence in other wavelength regions.

As expected, the Raman spectral signature shows a dependence on the water layer thickness. For the Raman spectral band a background signal remains within the transmission bandpass of the filters when both quartz plates were in contact (layer thickness close to zero), which cannot be attributed to Raman scattering. One possible explanation for this signature may be broadband luminescence from the quartz plate during laser excitation of the sample. This signal contribution is not dependent on film thickness and therefore not due to tracer fluorescence or impurities in the water. In the imaging setup this contribution is eliminated by subtracting the background measured during laser excitation of the dry surface.

4.3 Thickness calibration

The calibration tool allows us to measure the dependence of both, the Raman and the tracer-LIF signal intensity as a function of water film thickness using the respective filters in front of the camera (cf. Fig. 1). Results for tracer/water solutions with different tracer concentrations (LIF) or pure water (Raman) are shown in Fig. 10(a) and (b), respectively. For each liquid layer thickness the spectrally integrated signal within the transmission bandpass for LIF and Raman were spatially averaged in a rectangular region of interest (ROI) with homogeneous beam intensity. To investigate the possible influence of absorption of the excitation laser and signal trapping, respectively, measurements were repeated at tracer concentrations of 0.1, 0.5 and 1.0% by weight. For all three data sets, the LIF intensity increases monotonically with layer thickness. In case of higher tracer concentrations the curves start to deviate from linearity at larger film thicknesses (as indicated in Fig. 10 below), indicating laser beam attenuation (cf. Fig. 6). Signal trapping can be neglected because of the much reduced absorption cross section at the fluorescence wavelengths (cf. Fig. 4). Due to this limitation, for the layer thickness range up to 500 µm all measurements presented in the following were performed with a tracer concentration of 0.1 wt%. For the later quantification of the LIF

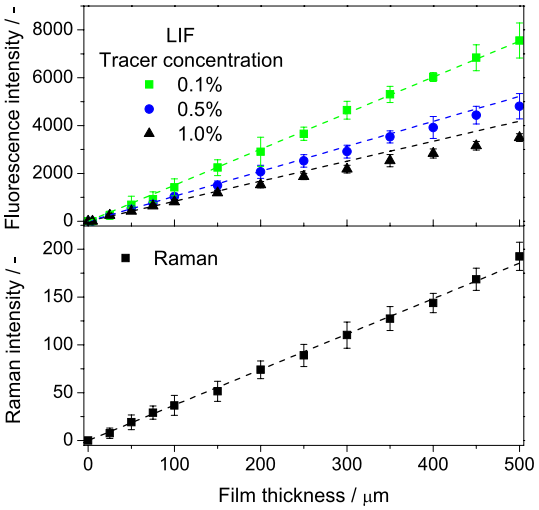

Fig. 10 Signal intensities vs. liquid film thickness evaluated from the recorded image data taken with the calibration tool in Fig. 2. *Symbols*: measurements (average value with $\pm 1\sigma$ rms error bars). *Upper panel*: fluorescence intensity for three tracer concentrations; *dashed lines* are linear fits to the data between 0–100 µm, with extrapolations to 500 µm. *Lower panel*: Raman intensities with a linear fit to all data points

and Raman signal the measured calibration data were fitted. In Fig. 10(a) the measured data points between 0 and 100 µm were linearly fitted and extrapolated up to thicknesses of 500 µm. For 0.1% tracer concentration a linear dependency is detected. At higher tracer concentrations the gap between measured signal and the linear fit is increasing with increasing film thickness due to laser attenuation inside the liquid layer.

With a simple model the effect of laser beam attenuation on the measured LIF signal intensity within the sample can be described. I_0 is the laser intensity entering the liquid, x is the distance from the entrance window, and σ_{abs} is the absorption cross section of the tracer at the laser wavelength. Thus, the intensity of the excitation laser at location x in the liquid layer with the tracer concentration n_{tr} can then be expressed via the Beer-Lambert law

$$I(x) = I_0 \exp(-n_{\mathrm{tr}}\sigma_{\mathrm{abs}}x) \tag{3}$$

When neglecting signal trapping, the fluorescence intensity, I_{LIF}, emitted towards the detector from the respective volume element is the integrated LIF intensity from $x = 0$ to the film surface $x = d$:

$$I_{\mathrm{LIF}}(d) = \eta\phi n_{\mathrm{tr}}\sigma_{\mathrm{abs}} \int_0^d I(x)\,dx \tag{4}$$

Using (3), this gives

$$I_{\mathrm{LIF}}(d) = \eta\phi I_0\big(1 - \exp(-n_{\mathrm{tr}}\sigma_{\mathrm{abs}}d)\big) \tag{5}$$

where η represents a detection efficiency of the experimental setup, and ϕ is the fluorescence quantum yield of the tracer. The attenuation of laser light is proportional to the number of tracer molecules inside the observation volume. For small concentrations the attenuation is negligible, but with an increasing number of tracer molecules laser energy decreases along the beam path, so that the fluorescence intensity does not follow the linear relationship anymore.

4.4 Film thickness imaging

In this section, we first discuss two-dimensional (2D) imaging measurements of liquid layers deposited on the quartz plate at room temperature, followed by experiments studying liquid layer evaporation at elevated temperatures.

Film thickness imaging was done using both, the tracer LIF and the Raman scattering method. Because these experiments were conducted for steady state conditions averaging of the acquired image files over 50 laser shots was possible for S/N improvement. Before each experiment the signal intensity is calibrated for a known layer thickness by placing the calibration tool at the position of the quartz plate and recording an image with a fixed plate separation (typically 400 µm). After the usual image processing steps (background subtraction, laser pulse energy correction) conversion to layer thickness was done with the previously derived calibration function after multiplying with a scaling factor obtained from the known liquid layer thickness measurement with the calibration tool.

Figure 11 shows the two image segments registered for the LIF (panel a) and Raman (panel b) detection channels through the image doubler from a droplet film deposited and spread manually on the quartz plate. It must be emphasized that the maximum pixel counts in both raw images are quite different due to the intrinsic weakness of the Raman scattering process. In the respective lower graphs a thickness profile is presented taken along the horizontal lines drawn in each image. The images from both detection channels are quite similar in shape and thickness distribution within the illuminated droplet area, confirming the appropriate scaling procedure from the calibration curves for both diagnostic methods. One observes for these droplet-like liquid layers a rather steep gradient of 180 µm/mm towards the edge of the droplet. Spurious fragments of smaller droplets are rare due to the careful placement of the main droplet on the plate.

To realize a situation more representative for practical systems the water/tracer solution was deposited on the quartz plate using the described nozzle setup with a single pulse ejection at a back pressure of 5 bar, when the injector was inclined by 45° with respect to the plate normal at a distance of approximately 50 mm from the plate. Figure 12 shows the obtained images for both detection channels. The spray enters the image region from the right in Fig. 12. Both images show a quite compact central area that is surrounded by a thin layer resulting from mist formation, especially on

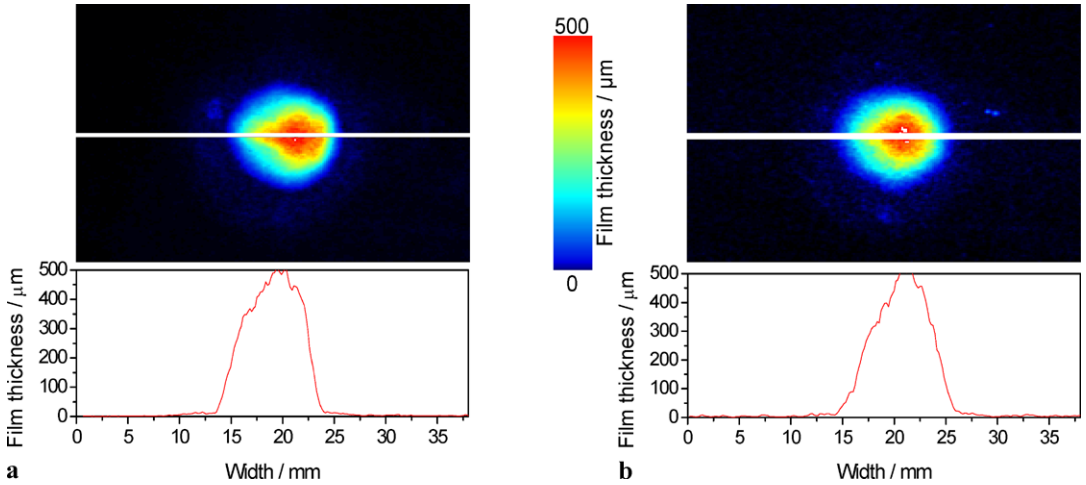

Fig. 11 Film thickness images (*upper row*) and thickness profiles along the *white lines* in the images (*lower row*), using tracer LIF (**a**) and Raman scattering (**b**), respectively. The films were generated by a pipette

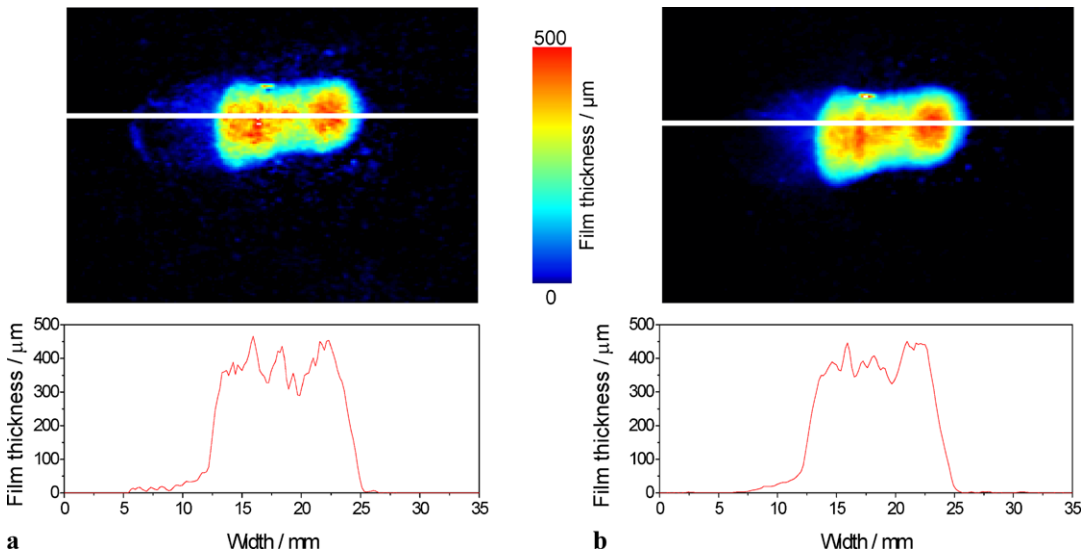

Fig. 12 Film thickness images (*upper row*) and thickness profiles along the *marked lines* in the images (*lower row*) using tracer LIF (**a**) and Raman scattering (**b**), respectively. The films were generated by a spray nozzle

the lee-side of the spray impingement position. The thickness profiles along the white horizontal lines illustrate these findings and show the large dynamic range of thicknesses that can be detected.

4.5 Film evaporation

The simultaneous LIF/Raman thickness imaging technique was also applied to a situation, where film evaporation takes place during the image-recording period. Again, the variation of layer thickness with time was evaluated inside a small ROI in the center of the deposited liquid layer. In contrast to the previous experiments the tracer-doped water sample now is exposed to the atmosphere for a fairly long period of time and preferential evaporation of the tracer can bias the thickness measurements due to a decreasing tracer concentration with time. In this case, the LIF signal will not only be a function of fluid film thickness but will be influenced by the time-dependent tracer concentration. Using the image doubler the current experimental setup provides the possibility for direct comparison between the tracer-based LIF and tracer-free Raman scattering measurements.

To speed up the liquid film evaporation the measurements were performed at a temperature of the liquid of approx. 60°C. Experiments were performed with two tracer species, ethyl acetoacetate (EAA) and acetone (AC) with different boiling points (180 and 56°C, respectively) resulting in a variation of the tracer volatility in the aqueous solutions. De-

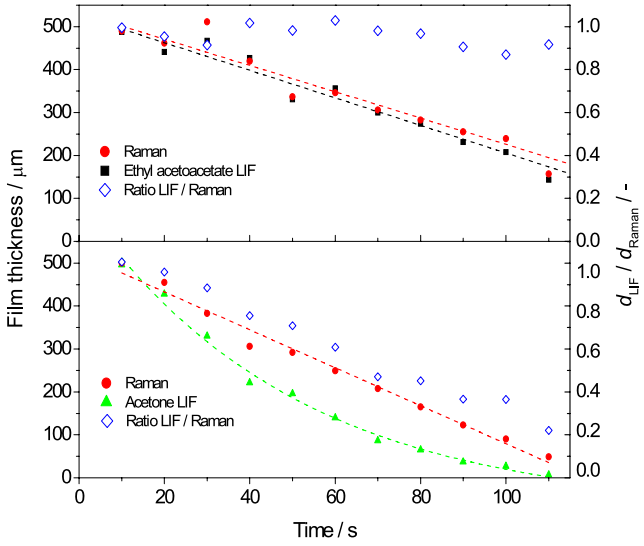

Fig. 13 Temporal evolution of liquid layer thickness from evaporating tracer-seeded water films by simultaneously processing the respective tracer LIF (*filled triangles* and *squares*, respectively) and Raman (*filled circles*) images. Tracer substance: EAA (*upper panel*), acetone (*lower panel*). *Open symbols*: thickness ratios, $d_{\mathrm{LIF}}/d_{\mathrm{Raman}}$

spite the high boiling point of EAA, equilibrium calculations predict a preferential evaporation for both cases.

Experiments were carried out with 0.1 wt% tracer concentration in both cases. Figure 13 shows the decreasing film thickness as a function of time when processing a 5×5 pixel interrogation region, which corresponds to an area of approx. $1.0 \times 1.0\ \mathrm{mm}^2$. Figure 13(a) depicts results using EAA as tracer, Fig. 13(b) shows the acetone results, both in comparison with the layer thickness derived from the respective Raman measurements. In the case of acetone the apparent layer thickness decreases faster than that determined from the Raman measurement, whereas the trends in thickness development deduced from the EAA tracer species more closely follows the Raman data.

The ratio of apparent thicknesses ($d_{\mathrm{LIF}}/d_{\mathrm{Raman}}$) derived from both methods can serve as an indicator for the deviation from proportionality to film thickness for the LIF signal relative to the Raman signal due to preferential evaporation, and is also plotted in each panel in Fig. 13 (open diamonds). It is observed that during the course of the experimental run this ratio stays close to unity for EAA for ∼75 s, while for acetone a significant decrease is visible almost from the beginning of the data acquisition. Due to the much higher vapor pressure and lower boiling point of acetone in comparison to EAA (cf. Table 1) evaporation of acetone from the solution will result in a correspondingly faster decay of the LIF signal, thereby biasing the thickness measurements to lower values with increasing time elapsed after start of experiment. Judging from the plotted ratios, deviations between the results from EAA-LIF and Raman imaging larger than 20% are noticeable after 120 seconds from start of data acquisition, while for the acetone measurements this value is already achieved after 30 seconds.

The experiments demonstrated that in these applications a simultaneous recording of a Raman scattering signal can help to perform an online calibration of the detected LIF signal in case selective evaporation (or photochemical degradation) of an added tracer might lead to a deviation of the evaluated LIF signal intensity from the calibration function determined in separate experiments where such deficiencies are not encountered. In the present experiments the possibility to simultaneously record LIF and Raman images of liquid layers enables one to correct these shortcomings, as long as a suitable tracer with co-evaporative properties is not available. Note that the slow evaporation process studied here can be considered as a bad-case scenario because the system has a chance to approach equilibrium compositions. In applications such as flash evaporation this effect might be reduced by a kinetic hindrance for preferential evaporation.

5 Outlook

So far, we presented a method for the determination of liquid water film thickness on transparent surfaces using the simultaneous and spatially resolved detection of tracer fluorescence and spontaneous Raman scattering, respectively. Although this is an ideal situation, in many practical systems optical access through transparent walls can be accomplished without significant disturbance of the operating conditions. For opaque walls excitation and detection from the same side would be required. In this case efficient suppression of scattered laser light and detection through high performance filters, and discrimination against unwanted inelastic luminescence from the wall will be the main challenges.

The effect of preferential tracer evaporation reported here constitutes a drawback for quantitative film thickness measurements based on tracer LIF, might be compensated by selecting a combination of two tracers with compensating evaporation behavior. In addition, as shown here, the simultaneous application of the tracer-based LIF and Raman techniques can be used with advantage to derive information about the evaporation history of tracer and solvent during film thickness measurements. The applicability of this approach is part of ongoing investigations.

In the present work, the Raman technique was applied for single component liquids and liquids that contain minute quantities of tracers only. For the more general and practically interesting cases of multicomponent mixtures, e.g., alcohol in water, the effect on density changes upon the preferential evaporation of one component must be considered. In this case the method would turn into a number density measurement for that specific component rather than

a layer thickness measurement. In addition, complications may arise from overlapping Raman bands from each component in the mixture. These challenges will be investigated in future work.

6 Summary and conclusions

Using laser excitation at 266 nm, spontaneous Raman scattering and tracer-based laser-induced fluorescence were applied simultaneously for the imaging measurement of the thickness of liquid water films on a transparent quartz plate.

The technique employs two-dimensional imaging with backward signal detection geometry. An intensified CCD camera was equipped with an image doubler that provides two spectrally filtered detection channels spatially separated on the CCD. Absolute signal intensities were calibrated with liquid layers of known thickness formed between two parallel quartz plates with adjustable distance. Experiments were presented where liquid droplets were spread on a transparent quartz plate, either manually or by water spray deposition through a commercial injection nozzle.

The tracer-free Raman method can provide a handle for correction of tracer-based LIF signal intensities that are biased due to non-ideal evaporation characteristics from the aqueous solution. It also allows a comparison of the behavior of different water/tracer systems under practical conditions and thus gives information about potential errors that occur from tracer-based LIF measurements. For practical applications the obvious advantages of the tracer-free Raman technique for imaging the thickness of liquid layers are compromised by low signal levels. The results emphasize the importance for the choice of a suitable tracer with volatility close to that of the solvent, and ethyl acetoacetate was shown to perform better in this respect than acetone.

Acknowledgements The authors acknowledge the financial support of the German research foundation (DFG) within the framework of GRK1114. We would like to thank Dirk-Peter Herten and coworkers (Bioquant, Univ. Heidelberg) for their cooperation and technical support in using their spectrometers. Calculations of vapor-liquid equilibria of multicomponent mixtures and fruitful discussions with M.A. Siddiqi (Univ. of Duisburg-Essen) are gratefully acknowledged.

References

1. G.P. Celata, M. Cumo, A. Mariani, L. Saraceno, Heat Mass Transf. **45**, 1029 (2009)
2. I. Gekas, P. Gabrielsson, K. Johansen, SAE Technical Paper 2002-01-0289 (2002)
3. L.W. Evers, K.J. Jackson, SAE Technical Paper 950002 (1995)
4. E.T. Hurlburt, T.A. Newell, Exp. Fluids **21**, 357 (1996)
5. T.A. Shedd, T.A. Newell, Rev. Sci. Instrum. **69**, 357 (1998)
6. M.C. Drake, T.D. Fansler, A.S. Solomon, G.A. Szekely, SAE Technical Paper 2003-01-0547 (2003)
7. P.G. Felton, D.C. Kyritsis, S.K. Fulcher, SAE Technical Paper 952464 (1995)
8. E. Kull, G. Wittafsky, W. Stolz, Opt. Lett. **22**, 645 (1997)
9. M. Alonso, P.J. Kay, P.J. Bowen, R. Gilchrist, S. Sapsford, Exp. Fluids **48**, 133 (2010)
10. W. Hentschel, A. Grote, O. Langer, SAE Technical Paper 972832 (1997)
11. A.A. Mouza, N.A. Vlachos, S.V. Paras, A.J. Karabelas, Exp. Fluids **28**, 355 (2000)
12. S. Wittig, J. Himmelsbach, M. Hallmann, W. Samenfink, A. Elsässer, MTZ, Motortech. Z. **55**, 160 (1994)
13. H. Yang, D. Greszik, T. Dreier, C. Schulz, Appl. Phys. B **99**, 385 (2010)
14. A. Schagen, M. Modigell, Exp. Fluids **43**, 209 (2007)
15. J. Wolfrum, T. Dreier, V. Ebert, C. Schulz, in *Encyclopedia of Analytical Chemistry*, ed. by R.A. Meyers (Wiley, Chichester, 2000)
16. K. Kohse-Höinghaus, R.S. Barlow, M. Aldén, J. Wolfrum, Proc. Combust. Inst. **30**, 89 (2005)
17. C. Schulz, V. Sick, Prog. Energy Combust. Sci. **31**, 75 (2005)
18. A.C. Eckbreth, *Laser Diagnostics for Combustion, Temperature and Species*, 2nd edn. (Gordon & Breach, Amsterdam, 1996)
19. J. Bartlett, K. Voss, Appl. Opt. **37**, 3324 (1998)
20. R.S. Barlow, P.C. Miles, Proc. Combust. Inst. **28**, 269 (2000)
21. W.F. Gregory, R.A. Copeland, Appl. Opt. **36**, 2686 (1997)
22. G.M. Hale, M.R. Querry, Appl. Opt. **12**, 555 (1973)
23. M.A. Siddiqi, *Institute for Combustion and Gasdynamics*. Univ. Duisburg-Essen, 2009, private communication
24. H. Xu, P.J. Wentworth, N.W. Howell, J.A. Joens, Spectrochim. Acta A **49**, 1171 (1993)
25. D.R. Lide, *CRC Handbook of Chemistry and Physics*, 86th edn. (Taylor & Francis, Boca Raton, 2005/2006)
26. Beilstein CrossFire Database, Elsevier Properties S.A., ©2007–2009